Electronic Supplementary Information

Influence of Cu insertion on the thermoelectric properties of the quaternary cluster compounds $Cu_3M_2Mo_{15}Se_{19}$ (M = In, K) and $Cu_4In_2Mo_{15}Se_{19}$

Patrick Gougeon[1,*], Philippe Gall[1], Shantanu Misra[2], Adèle Léon[2], Christine Gendarme[2], Sylvie Migot[2], Jaafar Ghanbaja[2], Soufiane El Oualid[2], Bertrand Lenoir[2], Christophe Candolfi[2,*]

[1] *Sciences Chimiques de Rennes, UMR 6226 CNRS – Ecole Nationale Supérieure de Chimie de Rennes – Université de Rennes 1, Avenue du Général Leclerc, 35042 Rennes, France*

[2] *Institut Jean Lamour, UMR 7198 CNRS – Université de Lorraine, Campus ARTEM, 2 allée André Guinier, BP 50840, 54011 Nancy, France*

[*]Contact authors: patrick.gougeon@univ-rennes1.fr ; christophe.candolfi@univ-lorraine.fr

Content

Figure S8. EDXS-STEM elemental maps for $Cu_4In_2Mo_{15}Se_{19}$.

Figure S9. Magnetic field dependences of the Hall resistivity ρ_H for the $Cu_3In_2Mo_{15}Se_{19}$ and $Cu_4In_2Mo_{15}Se_{19}$ compounds and of the transverse electrical resistivity ρ_{xy} for $Cu_3K_2Mo_{15}Se_{19}$.

Figure S10. Temperature dependence of the hole concentration p_H for the $Cu_3In_2Mo_{15}Se_{19}$ and $Cu_4In_2Mo_{15}Se_{19}$ compounds.

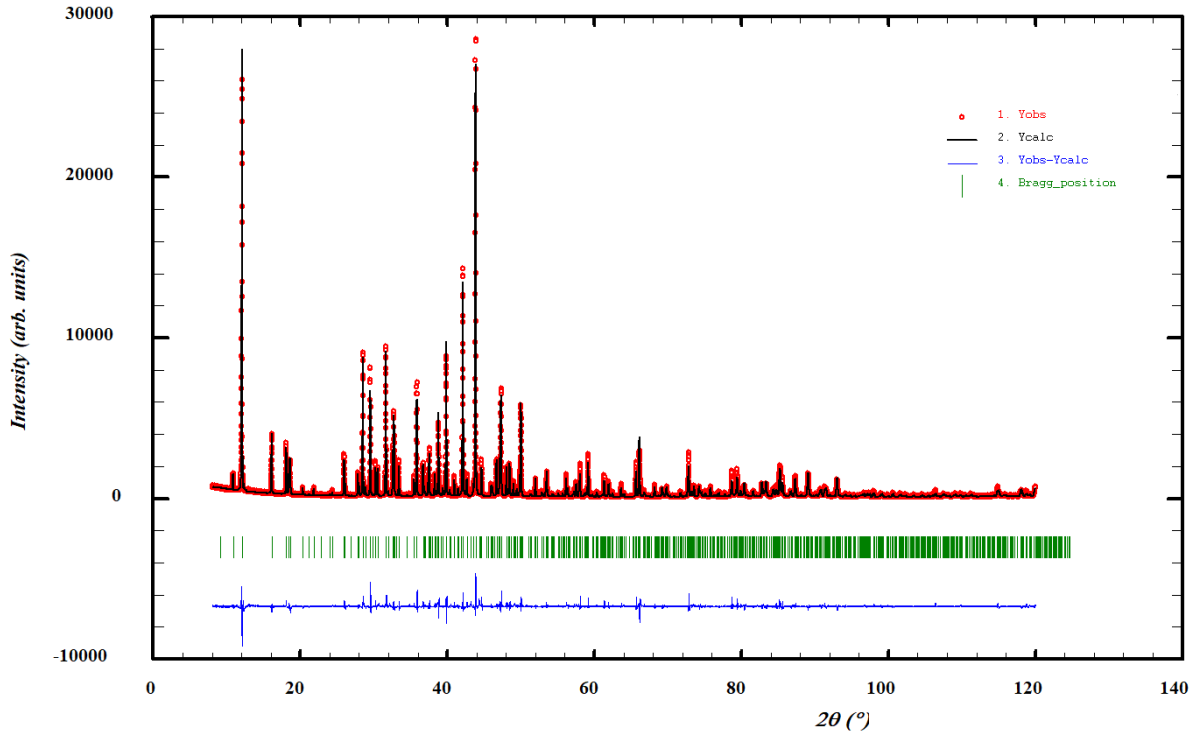

Figure S1. Rietveld refinement plot showing the observed, calculated and difference patterns of $Cu_3In_2Mo_{15}Se_{19}$.

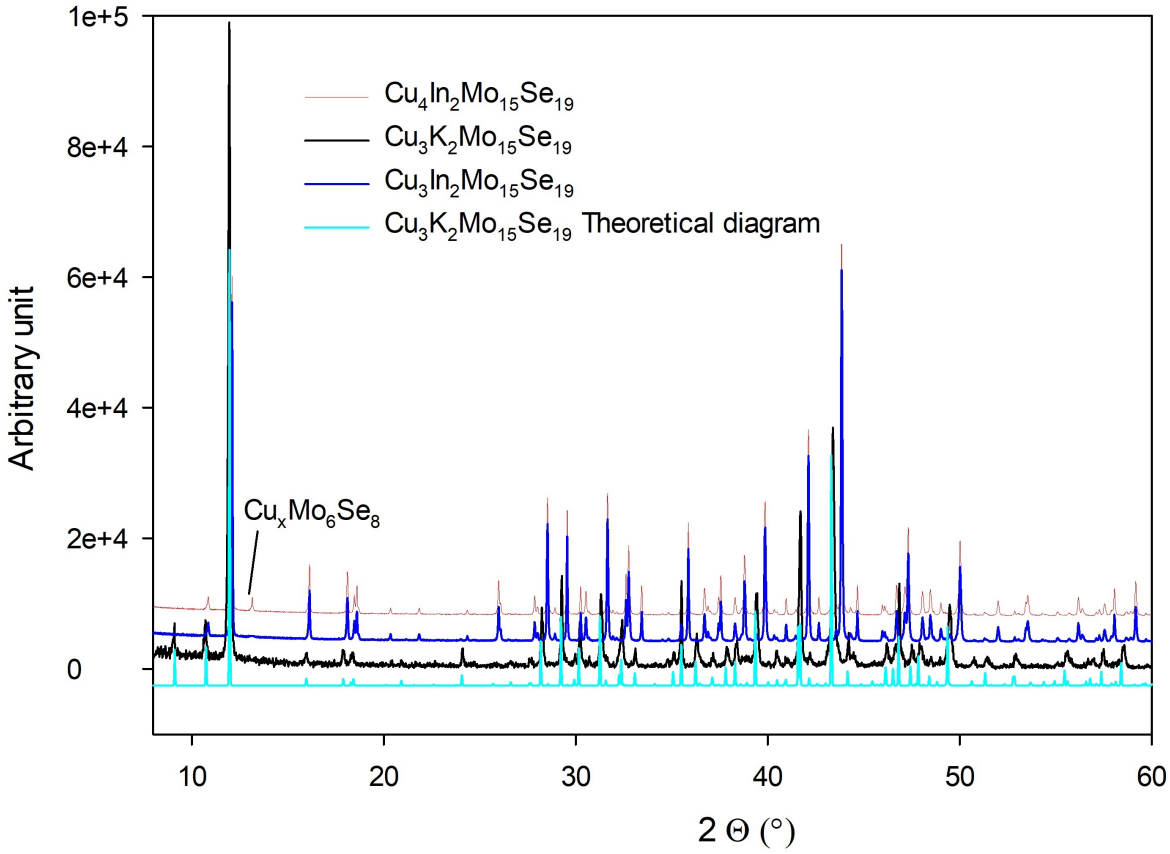

Figure S2. Experimental PXRD patterns at 300 K for the $Cu_3In_2Mo_{15}Se_{19}$, $Cu_4In_2Mo_{15}Se_{19}$, $Cu_3K_2Mo_{15}Se_{19}$ compounds and theoretical one for $Cu_3K_2Mo_{15}Se_{19}$.

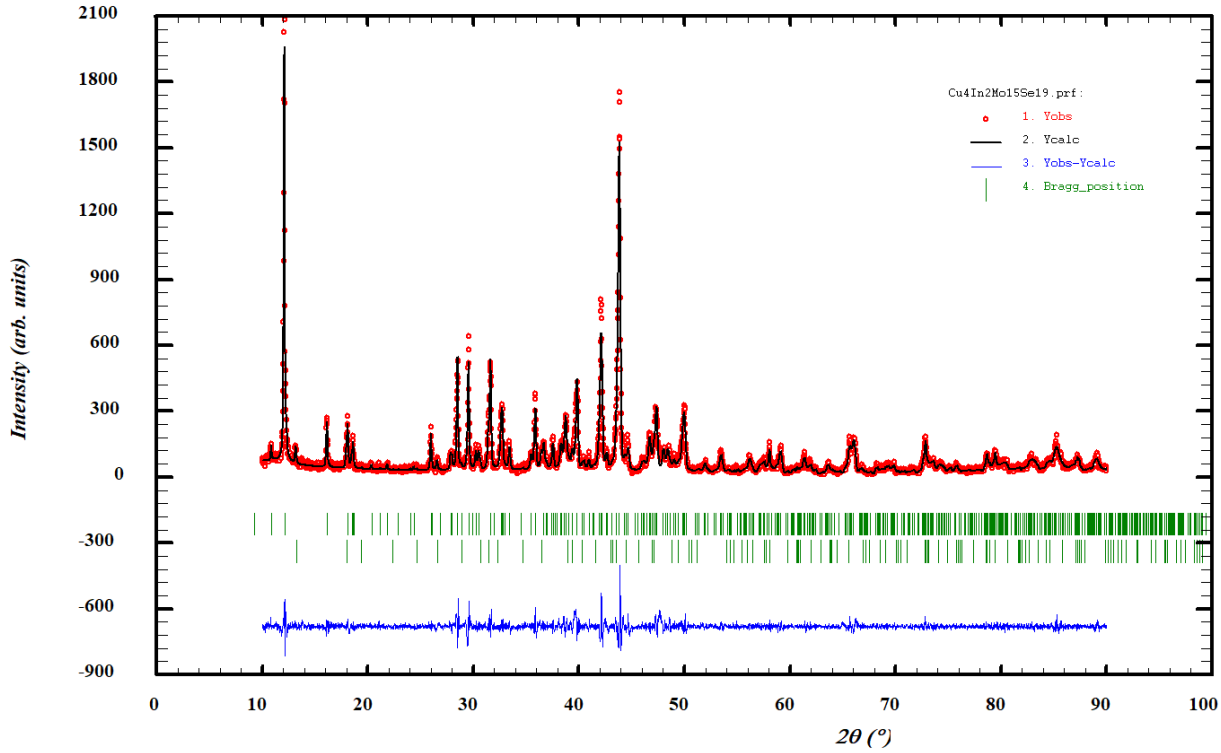

Figure S3. Profile matching mode refinement plot of $Cu_4In_2Mo_{15}Se_{19}$ (upper green vertical markers) and $Cu_xMo_6Se_8$ (lower green vertical markers).

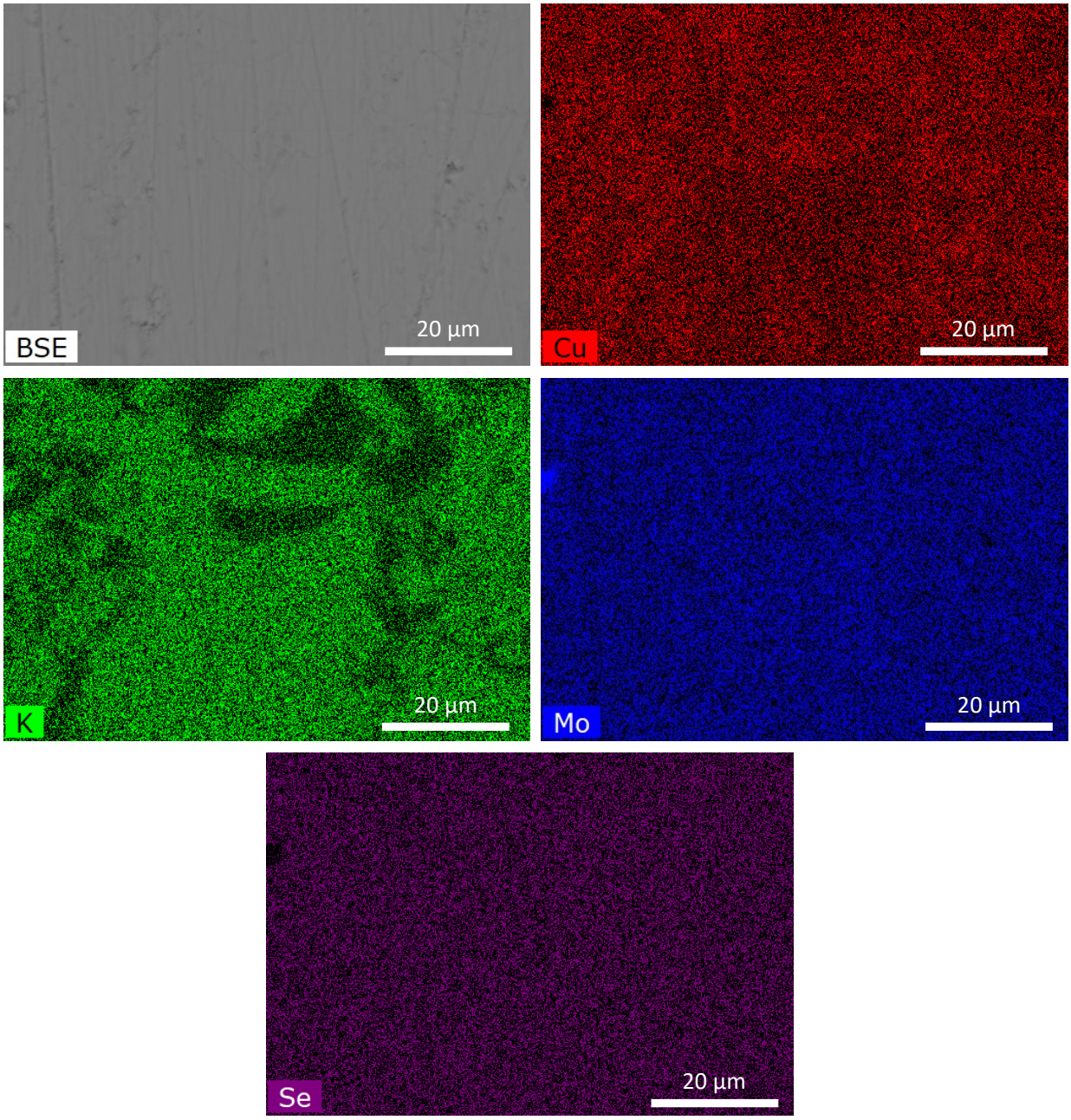

Figure S4. SEM image in backscattered electron mode (BSE) and its corresponding elemental X-ray maps for $Cu_3K_2Mo_{15}Se_{19}$.

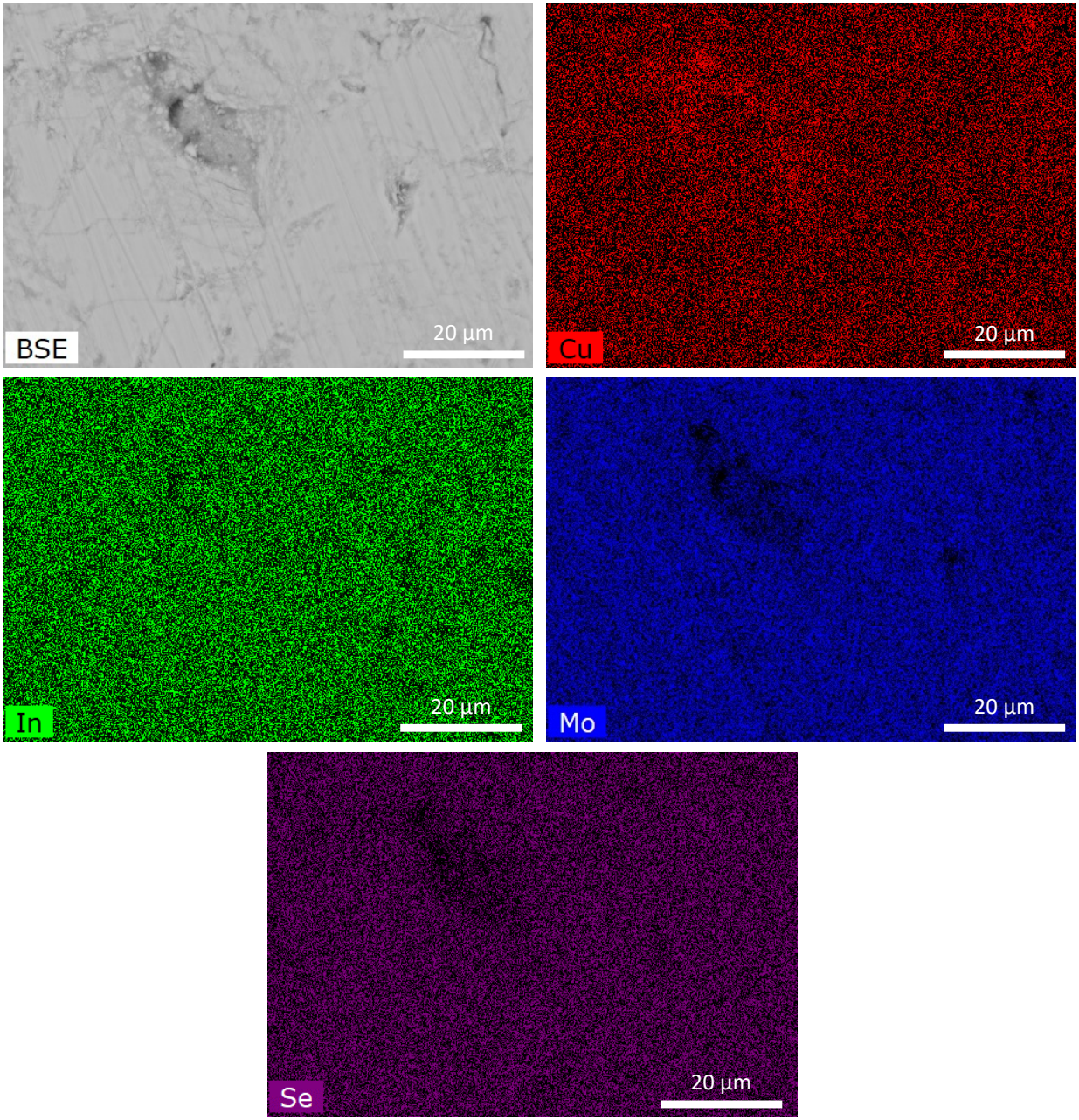

Figure S5. SEM image in backscattered electron mode (BSE) and its corresponding elemental X-ray maps for $Cu_3In_2Mo_{15}Se_{19}$.

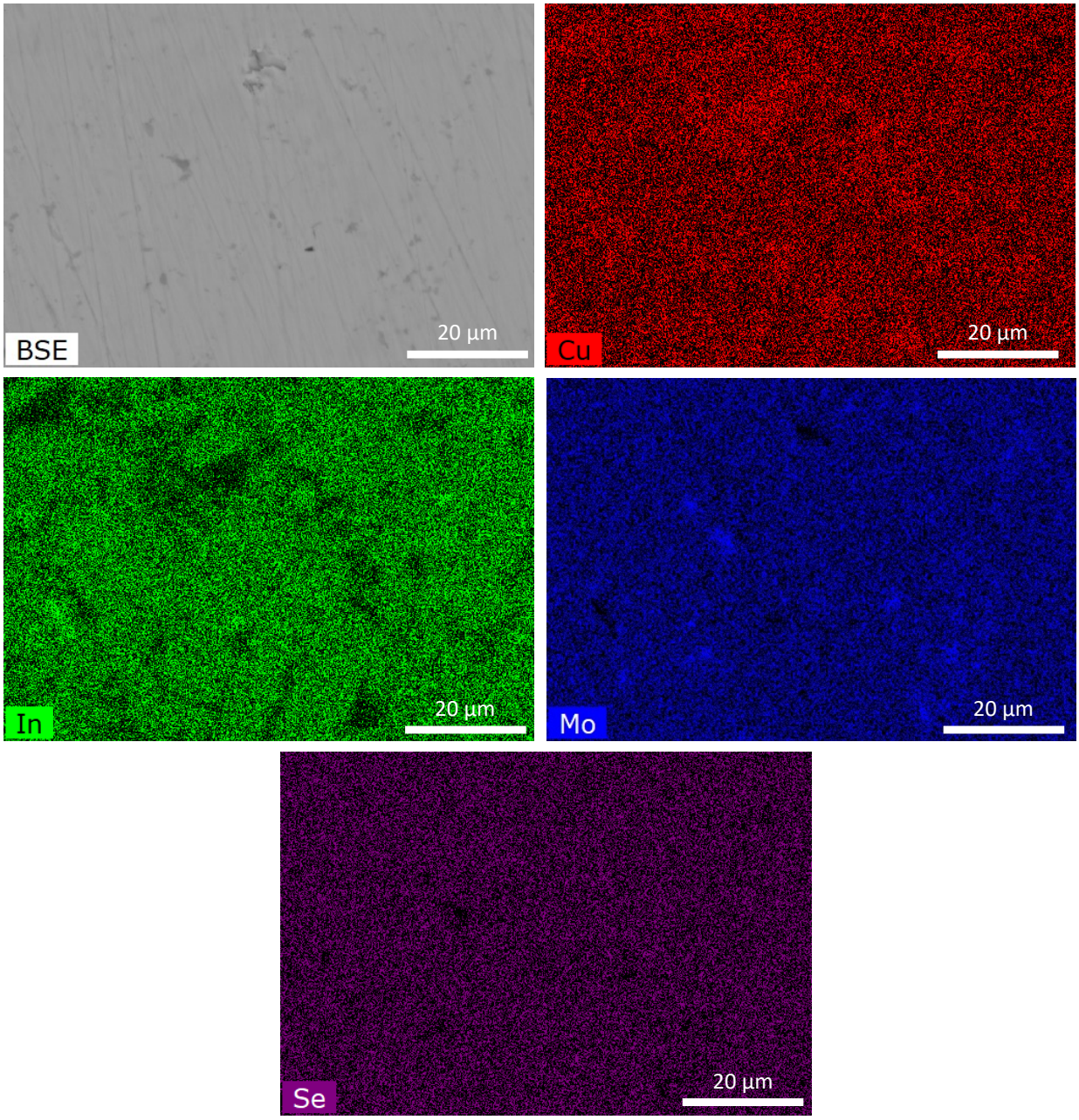

Figure S6. SEM image in backscattered electron mode (BSE) and its corresponding elemental X-ray maps for $Cu_4In_2Mo_{15}Se_{19}$.

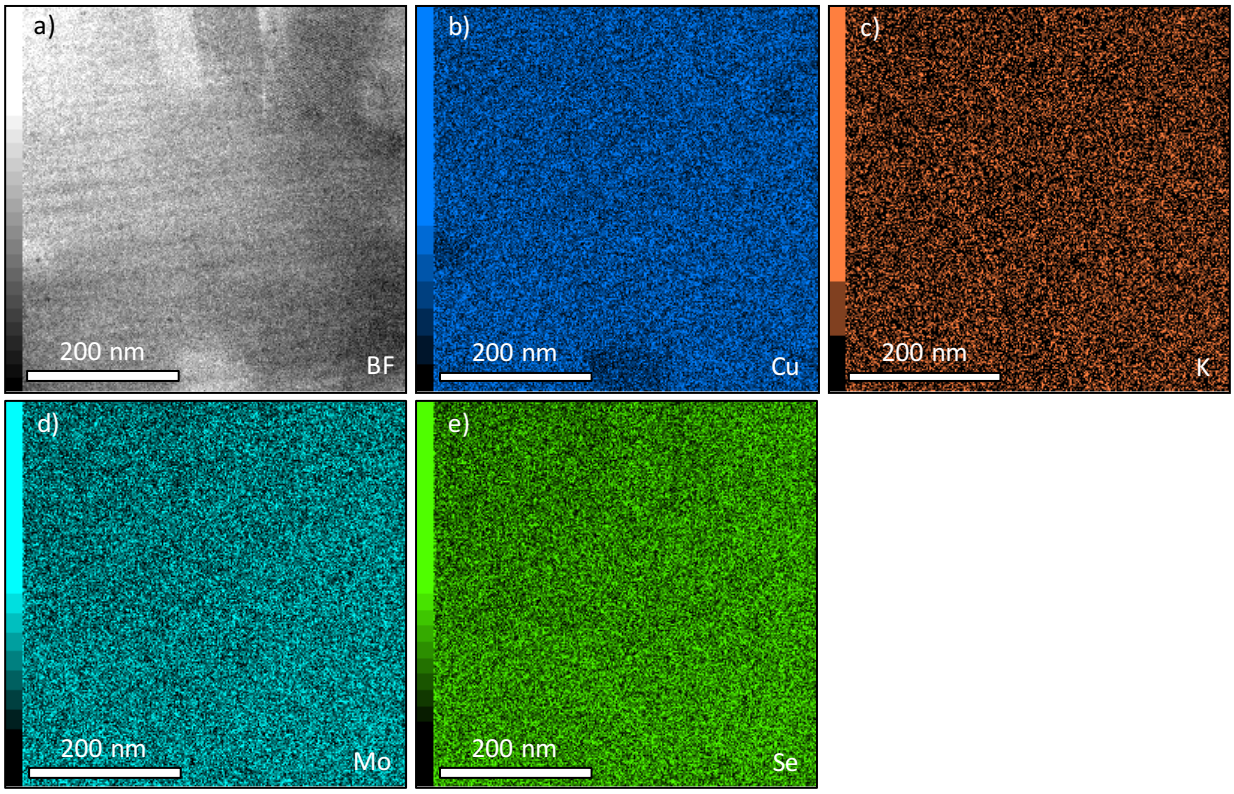

Figure S7. Bright-field image (BF, panel a) and corresponding elemental X-ray maps (panels b, c, d and e) obtained by scanning transmission electron microscopy (STEM) for $Cu_3K_2Mo_{15}Se_{19}$.

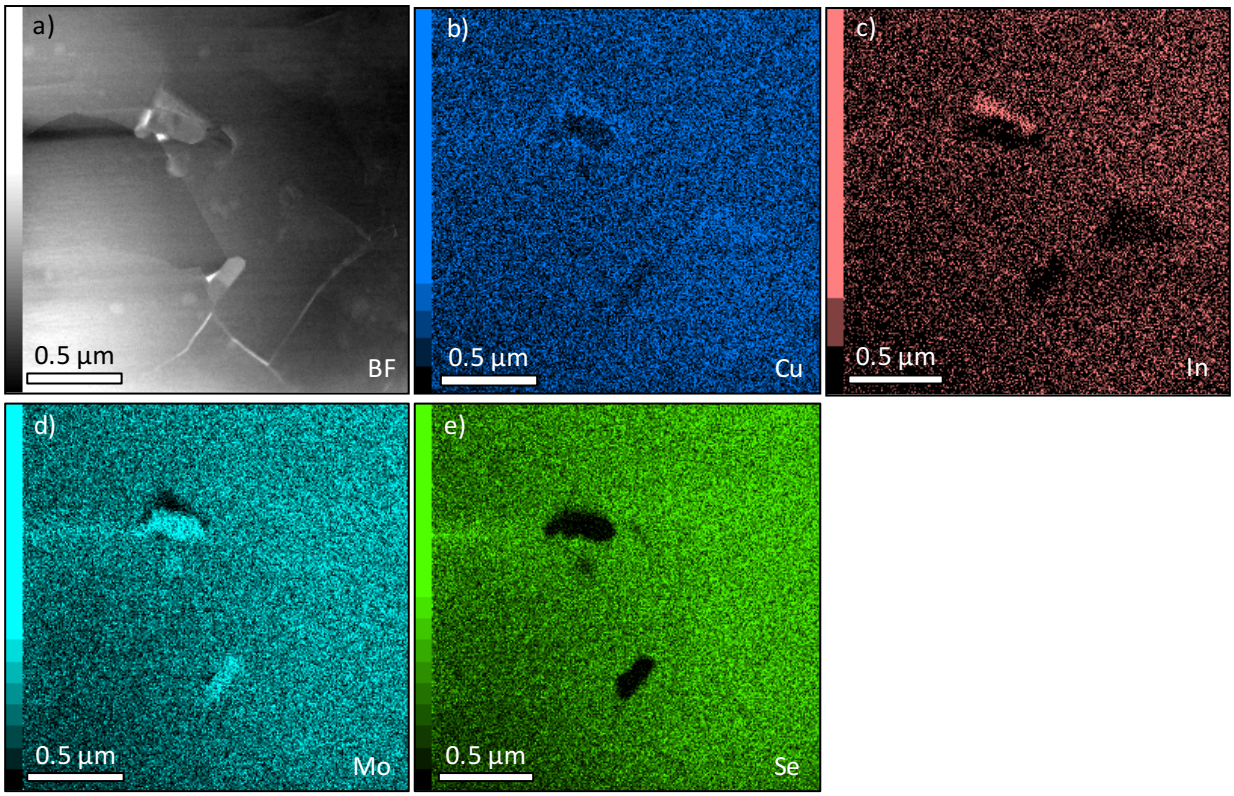

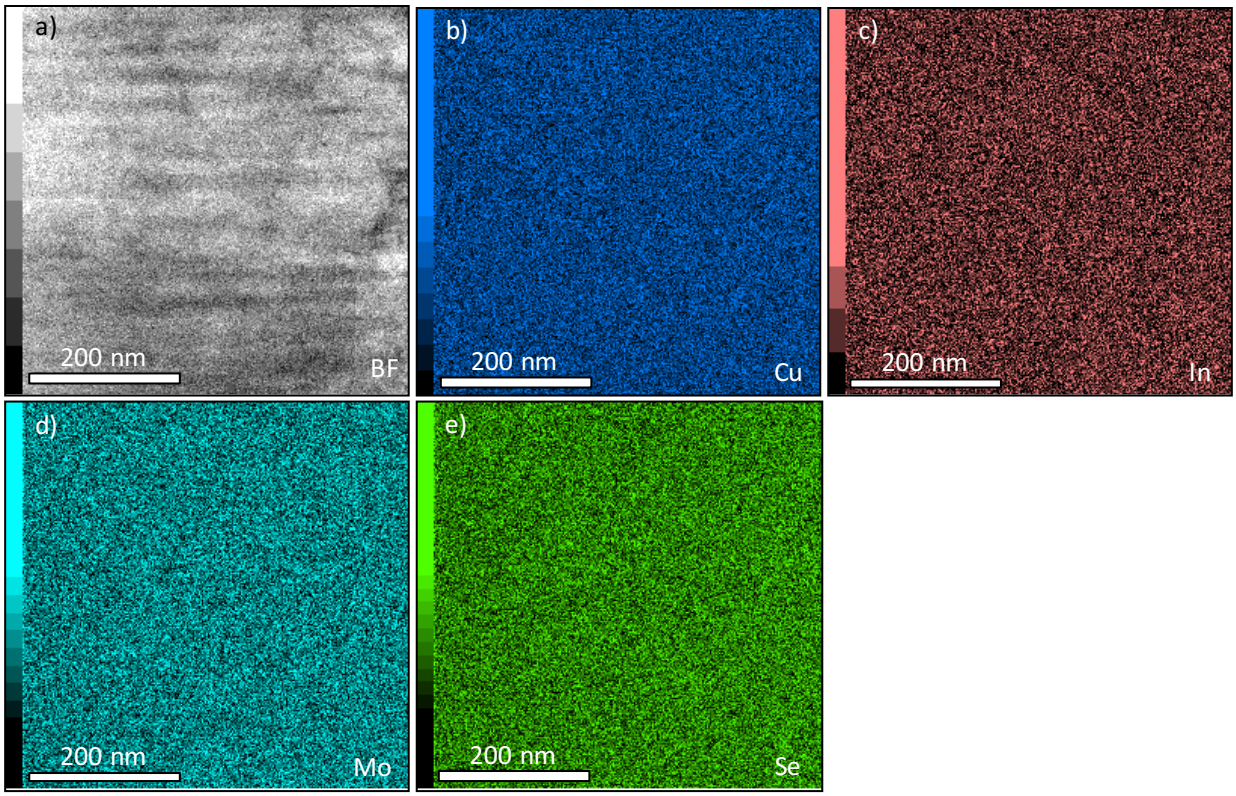

Figure S8. Bright-field image (BF) and corresponding elemental X-ray maps obtained by scanning transmission electron microscopy (STEM) for $Cu_4In_2Mo_{15}Se_{19}$ at two different scales. The top panels show the presence of minute amounts of In-rich and Mo-rich phases.

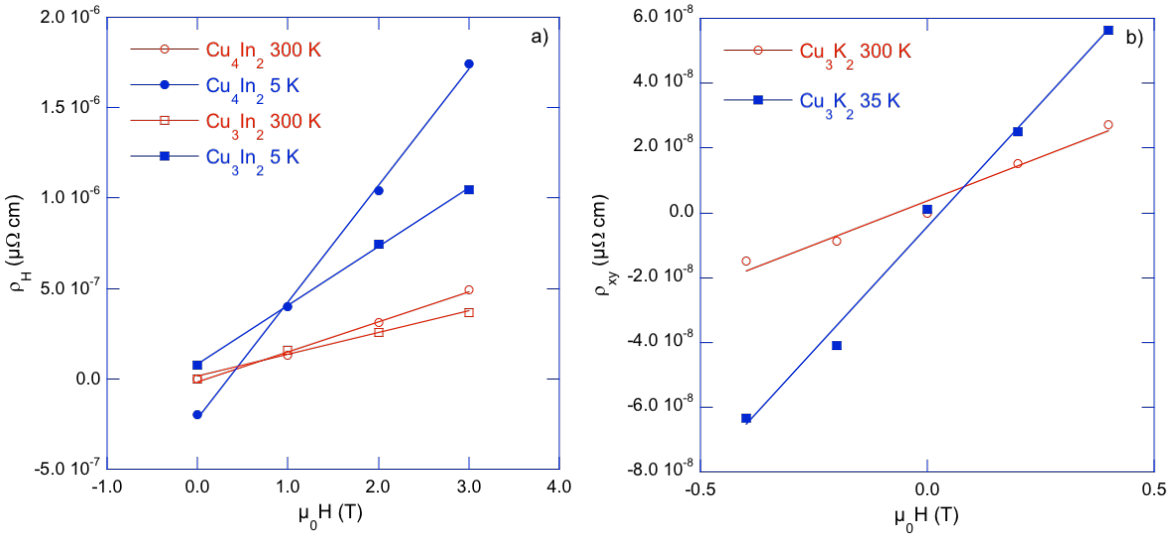

Figure S9. a) Magnetic field dependence of the Hall resistivity ρ_H at 300 and 5 K for the $Cu_3In_2Mo_{15}Se_{19}$ and $Cu_4In_2Mo_{15}Se_{19}$ compounds. b) Magnetic field dependence of the transverse electrical resistivity ρ_{xy} for $\mu_0 H \rightarrow 0$ at 300 and 35 K for $Cu_3K_2Mo_{15}Se_{19}$. In both panels, the solid lines stand for the best linear fits to the data.

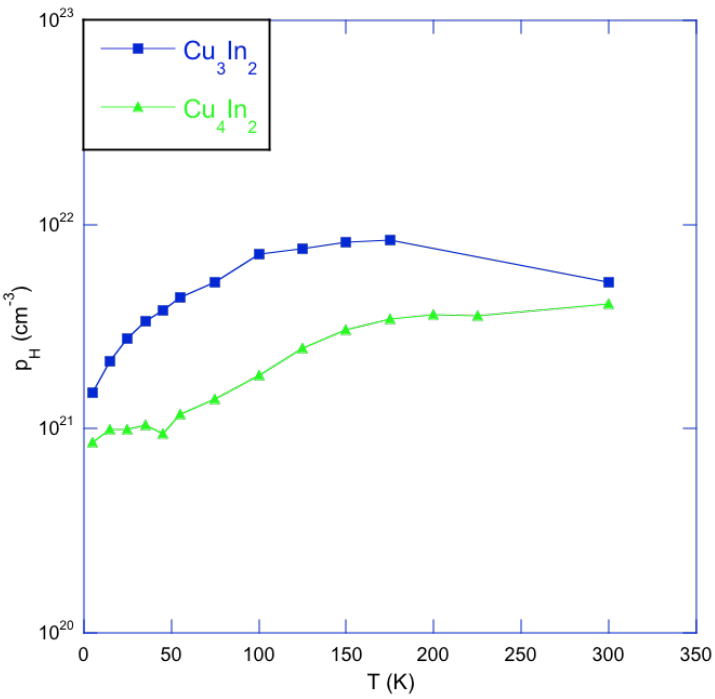

Figure S10. Temperature dependence of the hole concentration p_H for the $Cu_3In_2Mo_{15}Se_{19}$ and $Cu_4In_2Mo_{15}Se_{19}$ compounds. The solid lines are guides to the eye. The p_H values for $Cu_3K_2Mo_{15}Se_{19}$ could not be determined reliably as a function of temperature due to the pronounced metallic character of this sample giving rise to very low Hall signals, difficult to resolve experimentally.